Society of Medical Education & Research

2026, Volume 6, Issue 1, Page No: 60-77

ISSN: 3108-4834

Archive of International Journal of Cancer and Allied Science

Nuclear circPHLPP2 Facilitates ILF3-Dependent IL36γ Transcription to Drive Immune Evasion and Anti-PD-1 Resistance in Colorectal Cancer

Daniel Kim[1]*, Jihoon Park[1], Min-seo Kang[2], Hyun-woo Jung[3]

[1]Department of Colorectal Cancer and Circular RNA Biology, College of Medicine, Kyung Hee University, Seoul, South Korea.

[2]Department of Immune Evasion and PD-1 Resistance, College of Medicine, Chung-Ang University, Seoul, South Korea.

[3]Department of Nuclear Noncoding RNA and Transcription, College of Medicine, Kangwon National University, Chuncheon, South Korea.

***E-mail** ✉ jaesung.kim@khu.ac.kr

Abstract

The majority of patients with colorectal cancer (CRC) show only modest responses to anti-programmed cell death protein 1 (PD-1) treatment, and the precise reasons for this limited efficacy are not yet clear. Circular RNAs (circRNAs) are known to exert substantial influence on tumor formation and progression, offering possible utility in early detection and prediction of therapeutic outcomes. Nevertheless, investigations into the contribution of circRNAs to immune evasion in CRC remain scarce. Differential expression analysis of circRNA microarrays identified circPHLPP2. The association between circPHLPP2 levels and various clinicopathological parameters in CRC patients was assessed using RT-qPCR. Functional studies involving MTS assays, colony formation experiments, in vivo subcutaneous tumor models, and multicolor flow cytometry were conducted to clarify the role of circPHLPP2. Downstream molecular pathways were examined through RNA-seq, RT-qPCR, and Western blotting. Protein partners of circPHLPP2 were identified with RNA pull-down assays, RNA immunoprecipitation (RIP), and immunofluorescence staining. Expression of circPHLPP2 is elevated in CRC patients who do not respond adequately to anti-PD-1 therapy. This circRNA strongly drives CRC cell proliferation and accelerates tumor growth in experimental models. Silencing circPhlpp2 improves the antitumor activity of anti-PD-1 agents in vivo. At the mechanistic level, circPHLPP2 binds directly to ILF3, thereby promoting its nuclear accumulation. Nuclear ILF3 then augments IL36γ gene transcription, which in turn decreases the recruitment of NK cells into the tumor and suppresses their secretion of granzyme B and IFN-γ, ultimately supporting tumor advancement. In summary, this study identifies a previously unrecognized pathway by which a circRNA controls immune escape in CRC. circPHLPP2 represents a potential prognostic indicator and a candidate therapeutic target for improving outcomes in CRC patients.

Keywords: CircPHLPP2, Colorectal cancer, NK cell, Immune evasion

Introduction

Colorectal cancer (CRC) is the third most frequently diagnosed malignancy and the second leading contributor to cancer mortality across the world [1]. Patients with advanced-stage disease often face limited treatment options, which substantially impairs their quality of life and long-term survival [2]. The introduction of immune checkpoint inhibitors (ICIs), such as PD-1-blocking antibodies, has provided renewed optimism for managing advanced CRC. Clinical evidence indicates that pembrolizumab, a humanized anti-PD-1 monoclonal antibody, confers significant survival benefits in individuals with microsatellite instability-high or deficient mismatch repair (MSI-H/dMMR) advanced CRC [3]. However, patients whose tumors display microsatellite stability or proficient mismatch repair

Access this article online https://smerpub.com/

Received: 02 December 2025; **Accepted:** 14 Februaty 2026

How to cite this article: Kim D, Park D, Kang MS, Jung HW. Nuclear circPHLPP2 Facilitates ILF3-Dependent IL36γ Transcription to Drive Immune Evasion and Anti-PD-1 Resistance in Colorectal Cancer. Arch Int J Cancer Allied Sci. 2026;6(1):60-77. https://doi.org/10.51847/xKBvG5bTYx

(MSS/pMMR) — accounting for roughly 95% of all CRC cases — typically fail to benefit from single-agent ICI treatment [4, 5]. Encouraging progress has been reported with combined regimens, such as the pairing of anti-PD-1 antibodies and tyrosine kinase inhibitors (TKIs) in MSS/pMMR metastatic CRC, as observed in the REGONIVO study [6]. Despite these advances, reliable biomarkers to predict anti-PD-1 responsiveness in the predominant MSS/pMMR population remain lacking. It is therefore essential to deepen our understanding of the molecular basis of immunotherapy resistance to discover new predictive markers and actionable targets that can guide more individualized treatment strategies and improve patient survival.

Circular RNAs (circRNAs) constitute a class of stable, covalently closed single-stranded RNA transcripts that display widespread yet tissue-specific distribution in human cells [7]. Extensive profiling has revealed pronounced dysregulation of many circRNAs in CRC tissues, cell lines, peripheral blood, and exosomes, where they participate in key processes including tumor initiation, metastatic spread, and resistance to chemotherapeutic agents [8, 9]. Emerging data further implicate circRNAs in shaping the tumor immune landscape and enabling cancer cells to evade immune surveillance [10, 11]. For instance, exosomal CircCCAR1 has been shown to induce CD8+ T-cell exhaustion by stabilizing PD-1, contributing to anti-PD-1 resistance in hepatocellular carcinoma [12]. In gastric cancer, CircDLG1 fosters disease progression and anti-PD-1 resistance via upregulation of CXCL12 [13]. Despite these observations, the precise links between circRNAs and immunotherapy resistance in CRC have received limited attention. Owing to their structural stability and detectability in bodily fluids, circRNAs also hold considerable promise as noninvasive biomarkers for anticipating responses to anti-PD-1 therapy. Consequently, systematic exploration of circRNAs that drive immune evasion and therapeutic resistance in CRC is a high-priority research direction.

Natural killer (NK) cells represent critical components of the innate immune system, capable of recognizing and eliminating tumor cells without prior priming [14]. Beyond direct tumor cell lysis through perforin release and antibody-dependent cellular cytotoxicity (ADCC), NK cells secrete various cytokines and chemokines that recruit and stimulate T-cell responses, thereby linking innate and adaptive immunity [15, 16]. Tumors can counteract NK cell activity through diverse evasion tactics [17], including increased expression of inhibitory checkpoints such as PD-1 on NK cells. Therapeutic blockade of PD-1/PD-L1 signaling has been found to elicit potent NK cell activation, highlighting the importance of NK cells in achieving maximal benefit from immunotherapy [18]. Clinical and experimental evidence consistently links higher NK cell abundance in blood or tumor tissue with reduced metastatic potential and better prognosis in multiple malignancies, including CRC [17, 19]. Although NK cells are viewed as essential players in combinatorial cancer immunotherapy [20], the mechanisms responsible for anti-PD-1 resistance in CRC — especially those centered on NK cell dysfunction — are still incompletely understood.

The current work establishes that circPHLPP2 is markedly overexpressed in CRC tissues and correlates with resistance to anti-PD-1 therapy and inferior clinical outcomes. Mechanistically, circPHLPP2 interacts with ILF3 to facilitate its nuclear enrichment, thereby enhancing IL36γ transcription. The resulting IL36γ upregulation restricts NK cell infiltration into the tumor microenvironment. It attenuates their production of key effector molecules, including granzyme B and interferon-γ (IFN-γ), thereby promoting CRC development. Notably, genetic interference with circPHLPP2 significantly potentiates the therapeutic effect of anti-PD-1 treatment in preclinical models, supporting circPHLPP2 as both a predictive biomarker and a viable molecular target to enhance anti-PD-1-based strategies in CRC management.

Materials and Methods

Human tissues

Tissue samples for RNA microarray profiling and quantitative real-time PCR were collected from patients with metastatic microsatellite-stable/proficient mismatch repair (MSS/pMMR) colorectal cancer (CRC). These individuals had undergone colonoscopic biopsy or palliative surgical procedures and were treated with PD-1 inhibitors at Sun Yat-sen University Cancer Center from August 2019 to October 2022. Therapeutic responses were classified according to RECIST 1.1 guidelines. Overall survival (OS) was defined as the interval from the commencement of anti-PD-1 antibody administration until death from any cause or the final follow-up visit. For immunohistochemical (IHC) evaluation, a separate set of 381 formalin-fixed, paraffin-embedded CRC specimens with complete

clinicopathological records was assembled from Sun Yat-sen University Cancer Center between January 2007 and December 2012, with appropriate patient consent. In this group, OS was determined from the time of curative surgery to death or the most recent contact.

CircRNA microarray assays

To uncover circRNAs potentially contributing to anti-PD-1 resistance in MSS/pMMR CRC, microarray analysis was performed on samples from 8 patients who achieved a partial response (PR) and 10 patients who progressed (PD) during anti-PD-1 treatment. Both tumor tissues and paired adjacent nontumor tissues were examined.

Sample processing and array hybridization were executed strictly according to Arraystar's standard protocols (Rockville, MD, USA). Linear RNAs were first degraded using RNase R to enrich for circRNAs. The remaining circRNAs were amplified and converted into fluorescently labeled cRNA via random priming using the Arraystar Super RNA Labeling Kit. Hybridization was carried out on the Human circRNA Array V2 (8 × 15 k, Arraystar). Scanned images were acquired with an Agilent Scanner G2505C and processed using Agilent Feature Extraction software (version 11.0.1.1). Subsequent quantile normalization and statistical analyses were conducted in the R environment.

Plasmid and cell transfection

The human circPHLPP2 (hsa_circ_0003681) overexpression construct was generated in the pLC5-ciR vector by GeneSeed (Guangzhou, China). An EIF4A3 overexpression plasmid was prepared in the pLVX vector by Tsingke Biotech (Beijing, China). Small interfering RNAs (siRNAs) targeting EIF4A3, HNRNPC, and U2AF2, together with their scrambled controls, were supplied by Genecefe (Jiangsu, China). siRNAs against ILF3 and the matching negative control were obtained from the Public Protein/Plasmid Library (Nanjing, China). Short hairpin RNA (shRNA) constructs directed against hsa_circ_0003681, mmu_circ_0014549 (mouse circPhlpp2), mouse IL36γ, and their negative controls were synthesized by GeneChem (Shanghai, China). Lentiviral vectors expressing mmu_circ_0014549 and the corresponding control were produced by GenePharma (Shanghai, China). Transfections and viral transductions were performed following the suppliers' recommended protocols and established methods [21].

Immunohistochemistry (IHC) assays

IHC experiments were carried out using previously validated standard procedures [22]. Paraffin sections were deparaffinized, rehydrated, and treated with 3% H_2O_2 for 10 minutes to block endogenous peroxidase activity. Heat-induced antigen retrieval was performed in a pressure cooker using either sodium citrate or EDTA buffer at sub-boiling temperature for 10 minutes. Nonspecific sites were blocked with 10% fetal bovine serum for 1 hour at ambient temperature. Primary antibody incubation was performed overnight at 4 °C, followed by 1 hour of incubation with a biotinylated secondary antibody at room temperature. Antibodies employed included anti-IL36γ (1:200 dilution, Abclonal) and anti-NKp46 (3 μg/mL, R&D). Sections were counterstained with hematoxylin. Staining intensity was graded semi-quantitatively as 0 (none), 1 (weak), 2 (moderate), or 3 (strong). The composite IHC score was computed by multiplying the intensity grade by the percentage of positively stained cells.

Flow cytometry

Tumor tissues were enzymatically dissociated in serum-free RPMI 1640 medium containing collagenase IV (0.2 mg/ml, Sigma-Aldrich) and DNase I (0.05 mg/ml, Roche). Single-cell suspensions were generated using a GentleMACS Octo Dissociator (Miltenyi Biotec, Germany). Following Percoll gradient separation to enrich immune cells, samples were stained with a viability dye (Zombie, 1:500, BioLegend) and fluorophore-labeled antibodies against surface markers (1:200 dilution). Intracellular cytokine staining was performed after 4-hour stimulation with Cell Stimulation Cocktail (eBioscience) using intracellular-specific antibodies at 1:100 dilution. Samples were acquired on a CytoFLEX instrument (BD Biosciences, USA) and data were processed with FlowJo version 10 software (FlowJo LLC).

RNA immunoprecipitation (RIP) assays

RIP procedures utilized the Magna RNA-binding protein immunoprecipitation kit (Millipore). Before use, magnetic beads were incubated with target antibodies for 30 minutes at room temperature to facilitate conjugation. Antibodies included anti-ILF3 (5 μg, Proteintech) and anti-EIF4A3 (5 μg, Proteintech), while normal IgG served as the control. Harvested cells were lysed in RIP buffer supplemented with protease and RNase inhibitors. Lysates were then mixed with the antibody-conjugated

beads and incubated overnight at 4 °C under rotation. After washing, RNA was recovered from the bead complexes and quantified by RT-qPCR, with enrichment levels normalized to input controls.

GST pull-down assays

RNA-binding proteins interacting with circPHLPP2 were isolated through an MS2-tagged circRNA pull-down strategy [23]. Cells were co-transfected with MS2-circPHLPP2 (or empty MS2 control) and MS2-MCP-GST plasmids using Lipofectamine 3000. All constructs were sourced from GeneChem (Shanghai, China). Forty-eight hours later, cells were lysed in RIPA buffer. The resulting circPHLPP2-MS2-MCP-GST complexes were affinity-purified using glutathione Sepharose 4B beads (Thermo Fisher Scientific). Captured fractions were subsequently subjected to RT-qPCR, Western blot analysis, or mass spectrometry depending on the experimental objective.

Fluorescence in situ hybridization (FISH) assay and immunofluorescence staining

FISH was conducted with a specialized probe hybridization system (SA-Biotin, GenePharma, Shanghai, China). Custom Cy3-labeled probes targeting circPHLPP2 were designed and synthesized by GenePharma. HCT116 cells were fixed and permeabilized, then pre-hybridized before overnight incubation with the Cy3-circPHLPP2 probes at 37 °C. Following six washes in Buffer C, nonspecific binding was blocked with PBS containing 1% BSA and 0.05% Triton X-100 for 30 minutes at room temperature. Cells were next incubated with primary antibody (1:100) for 1 hour at room temperature, followed by Alexa Fluor 488-conjugated secondary antibodies (1:500, Invitrogen) for 45 minutes at 37 °C and DAPI nuclear staining (1:1000, GenePharma) for 15 minutes. Confocal microscopy images were captured using an LSM 880 system (ZEISS, Germany).

In vivo tumorigenesis assays

Immunodeficient NSG, BALB/c nude, and immunocompetent C57BL/6J and BALB/c mice were obtained from Vital River (Beijing, China). Subcutaneous tumors were established by injecting CRC cells (1.5×10^6 MC38; 5×10^5 CT26; 5×10^6 HCT116 or RKO) into the right flank of 6-week-old animals. Beginning one week post-inoculation, tumor size was monitored every 3 days, and volume was calculated as V = (width² × length)/2. When tumors reached roughly 200 mm³, tissues and blood samples were collected for flow cytometry. Treatment studies were initiated at a tumor volume of 100 mm³, with mice receiving intraperitoneal injections of 50 μg anti-PD-1 antibody (BioXCell) or PBS control every three days. NK cell depletion was performed by weekly intraperitoneal injection of 100 μL anti-asialo-GM1 (Cell Biolabs) in BALB/c mice or intravenous administration of 75 μg anti-NK1.1 (BioXCell) every three days in C57BL/6J mice. Depletion began one day before tumor implantation. Animals were sacrificed upon reaching ethical endpoints. Excised tumors were weighed, documented photographically, and prepared for paraffin embedding and histological sectioning.

Statistical analysis

All statistical evaluations were conducted using GraphPad Prism 9.0 and SPSS 25.0. Student's t-test analyzed two-group comparisons, whereas chi-square tests were applied for multiple-group analyses. Survival data were visualized with Kaplan-Meier curves and compared using the log-rank test. Significance levels are indicated as follows: *P < 0.05; **P < 0.01; ***P < 0.001; ****P < 0.0001.

Results and Discussion

High-level circPHLPP2 is associated with poor outcomes in anti-PD-1 resistant CRC patients

A circRNA microarray screen was performed on 18 matched pairs of primary tumor and adjacent normal tissues from MSS/pMMR colorectal cancer (CRC) patients receiving anti-PD-1 therapy, to identify transcripts associated with treatment response. In this group, 10 patients were classified as resistant based on progressive disease (PD) per RECIST 1.1 standards [24], while 8 patients were classified as responsive due to partial response (PR). Heatmap visualization identified 94 circRNAs with significantly elevated expression in the resistant tumor samples **(Figure 1a)** and 65 circRNAs upregulated in tumor versus normal tissues **(Figure 1b)**. The intersection of these lists highlighted hsa_circ_0003681, a previously uncharacterized transcript originating from the PHLPP2 gene, hereafter referred to as circPHLPP2 **(Figure 1c)**.

Validation in a larger cohort of 67 anti-PD-1-treated CRC patients using RT-qPCR confirmed markedly higher circPHLPP2 levels in resistant cases relative to

responsive ones **(Figure 1d)** and in tumor tissues compared with matched normal mucosa **(Figure 1e)**. Stratification of patients according to the median circPHLPP2 expression level revealed, through Kaplan-Meier analysis, that those with higher expression experienced significantly reduced overall survival **(Figure 1f)**. Collectively, these data indicate that circPHLPP2 is closely linked to disease advancement and the development of immune evasion in CRC.

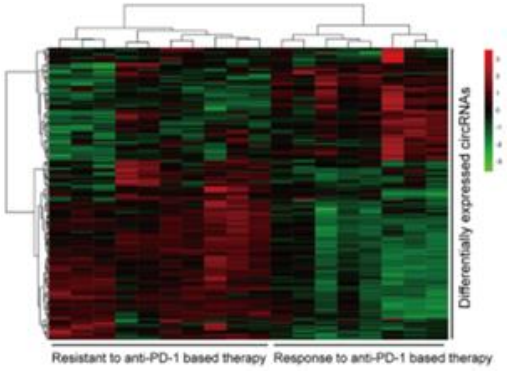

a)

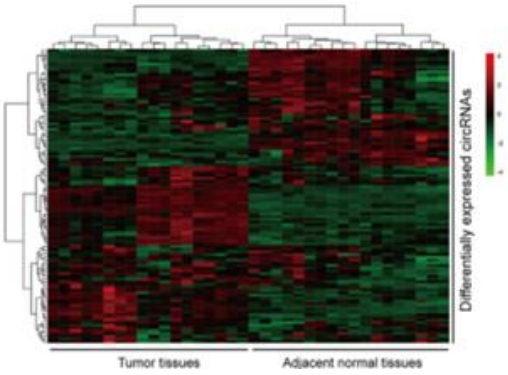

b)

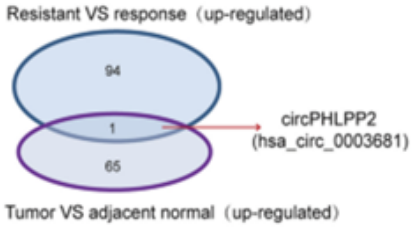

c)

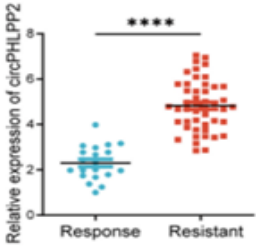

d)

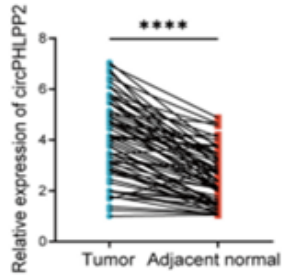

e)

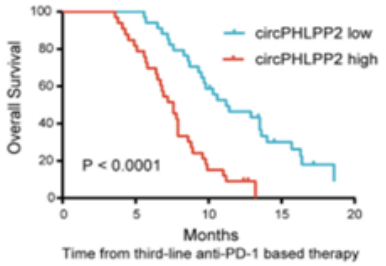

f)

g)

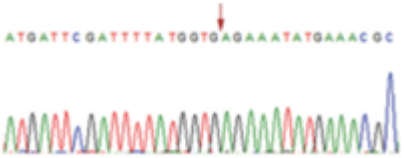

h)

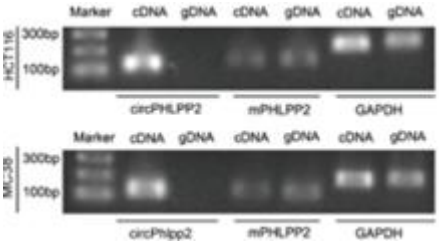

i)

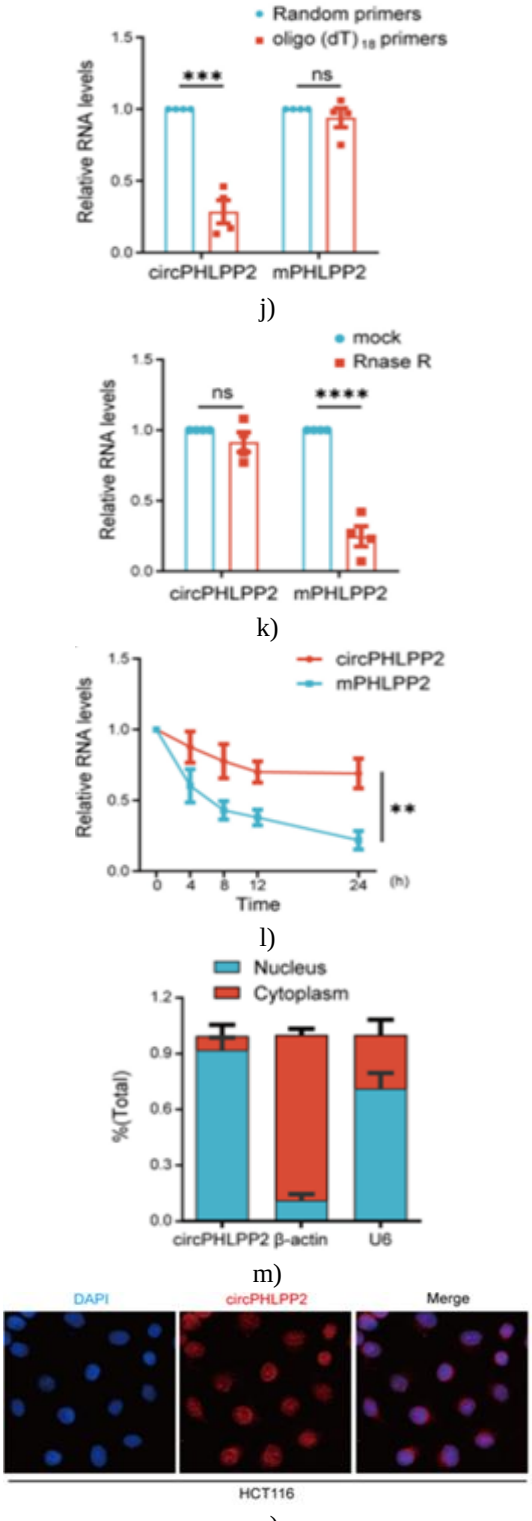

Figure 1. circRNA expression profiles in MSS/pMMR CRC and characterization of circPHLPP2

(a) Heatmap illustrating circRNA expression patterns in MSS/pMMR CRC tissues from patients resistant (n = 10) or responsive (n = 8) to anti-PD-1 therapy, (b) Heatmap of circRNA expression differences between MSS/pMMR CRC tumor tissues (n = 18) and paired adjacent normal tissues (n = 18), with thresholds set at Log2 (fold change) > 1 or < −1 and P < 0.05, (c) Venn diagram depicting the common circRNAs upregulated both in anti-PD-1-resistant samples and in CRC tumor tissues, (d) Expression levels of circPHLPP2 in anti-PD-1-resistant (n = 20) versus responsive (n = 47) tissues quantified by RT-qPCR, (e) circPHLPP2 expression in primary CRC tumors and matched adjacent normal tissues measured by RT-qPCR (n = 67), (f) Kaplan-Meier curves showing overall survival according to high versus low circPHLPP2 expression in CRC patients (n = 67, log-rank test), (g) Diagram depicting the generation of circPHLPP2 through back-splicing, (h) Confirmation of the back-splice junction sequence of circPHLPP2 by Sanger sequencing, (i) Detection of circPHLPP2 in HCT116 and MC38 cell lines via RT-qPCR and gel electrophoresis, (j) Comparison of circPHLPP2 and linear mPHLPP2 levels after reverse transcription using random hexamers or oligo(dT)18 primers, (k) Assessment of resistance of circPHLPP2 and linear mPHLPP2 to RNase R treatment by RT-qPCR, (l) Decay rates of circPHLPP2 and linear mPHLPP2 following Actinomycin D (2 μg/ml) exposure measured by RT-qPCR, (m) Determination of circPHLPP2 subcellular distribution using cytoplasmic/nuclear fractionation, and (n) Visualization of circPHLPP2 localization by FISH assay in HCT116 cells, with DAPI nuclear counterstaining. Statistical analysis for panels (d, e, j, and k) employed Student's t-test. Two-way ANOVA analyzed panel l. **P < 0.01, ***P < 0.001, ****P < 0.0001.

Characteristics of circPHLPP2 in CRC cells

Database interrogation in circBase (http://www.circbase.org/) revealed that circPHLPP2 is produced by back-splicing of exons 2 and 3 from the PHLPP2 locus on chromosome 16 (71736500–71748704), yielding a transcript 424 nucleotides in length **(Figure 1g)**. Divergent primers were used to amplify the distinctive backsplice junction, which was subsequently validated by Sanger sequencing **(Figure 1h)**. PCR using divergent primers successfully detected circPHLPP2 in cDNA but failed to produce a product from gDNA. In contrast, convergent primers amplified

the linear PHLPP2 isoform from both templates in HCT116 and MC38 cells **(Figure 1i)**. Amplification of circPHLPP2 occurred with random hexamer primers but not with oligo(dT)18 primers **(Figure 1j)**, consistent with the absence of a poly (A) tail. circPHLPP2 displayed pronounced resistance to RNase R digestion compared with linear PHLPP2 mRNA **(Figure 1k)**. Treatment with the transcriptional inhibitor Actinomycin D further confirmed the enhanced stability of circPHLPP2 relative to its linear counterpart **(Figure 1l)**. Subcellular fractionation and FISH experiments both demonstrated predominant nuclear localization of circPHLPP2 **(Figures 1m and 1n)**. These lines of evidence collectively confirm that circPHLPP2 is an authentic circular RNA molecule.

CircPHLPP2 promotes CRC progression in vivo

Functional investigation of circPHLPP2 in CRC involved the generation of overexpression constructs and backsplice-junction-specific siRNAs, with efficient modulation confirmed in cell lines. Interestingly, altering circPHLPP2 levels did not affect in vitro proliferative capacity or colony formation ability of human CRC cells, as shown by MTS and colony formation experiments **(Figures 2a-2f)**.

In vivo studies were performed by subcutaneously implanting modified CRC cells into NSG mice. These animals are severely immunodeficient, lacking mature T, B, and NK cells and incapable of immunoglobulin production [25]. Under these conditions, neither overexpression nor knockdown of circPHLPP2 influenced tumor xenograft growth **(Figure 2g)**. However, in BALB/c nude mice, which possess functional NK cells but lack mature T cells due to a Foxn1 mutation on chromosome 11 [26], circPHLPP2 overexpression substantially accelerated tumor development **(Figure 2h)**. In contrast, its depletion produced the opposite effect. These contrasting results in different host strains pointed to an immune-dependent mechanism, likely involving NK cells or B cells.

Consistent findings emerged when MC38 cells (MSI-H) with stable circPhlpp2 overexpression were inoculated into fully immunocompetent C57BL/6 mice, resulting in enhanced tumor growth **(Figure 2i)**. In the CT26 MSS model [27], circPhlpp2 overexpression led to a significant increase in final tumor weight, although the effect on growth kinetics did not reach statistical significance **(Figure 2j)**. Conversely, stable circPhlpp2 knockdown in both MC38 and CT26 lines strongly suppressed tumor expansion and markedly improved survival of tumor-bearing animals **(Figures 2k and 2l)**. Overall, these data indicate that circPHLPP2 exerts its tumor-promoting effects in CRC primarily by modulating the host immune microenvironment.

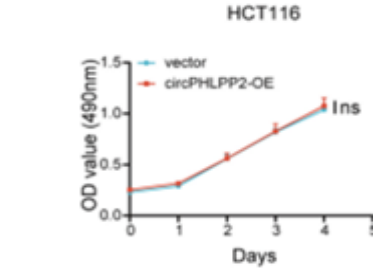

a)

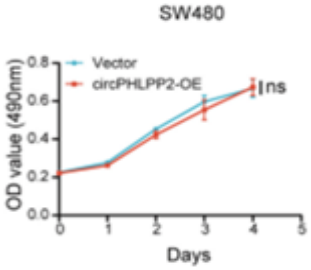

b)

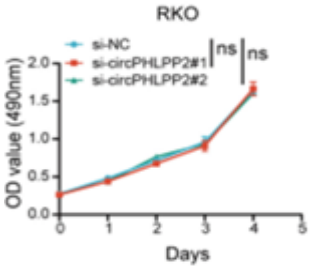

c)

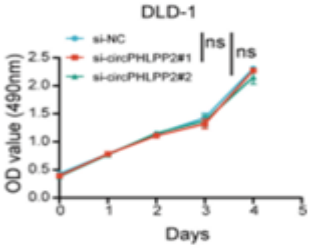

d)

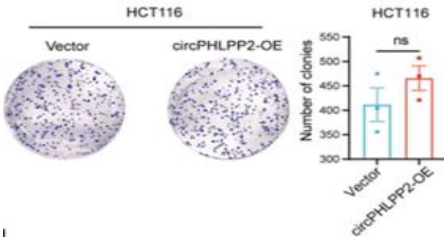

e)

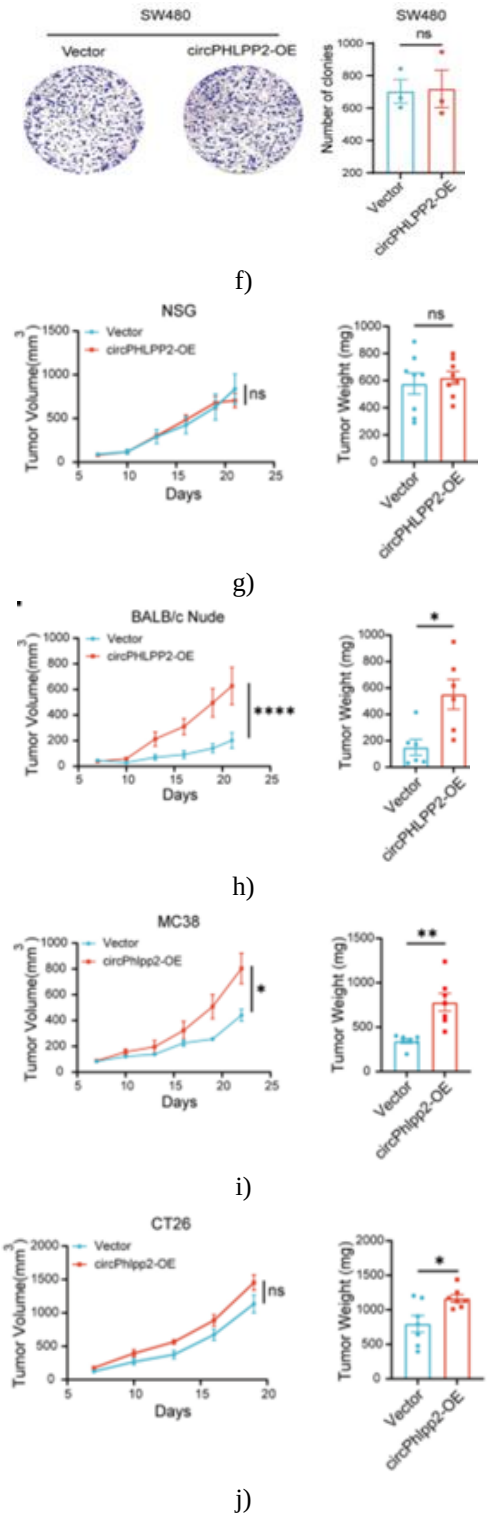

Figure 2. circPHLPP2 promotes proliferation of CRC cells in vivo

(a-d) Growth curves of CRC cells upon circPHLPP2 overexpression or silencing, evaluated using an MTS assay, (e and f)Results of colony formation assays in CRC cells with circPHLPP2 overexpression, (g) Tumor growth curves and final weights in NSG mice following subcutaneous implantation of HCT116 cells stably overexpressing circPHLPP2 (n = 8), (h) Tumor growth curves and final weights in BALB/c nude mice after implantation of HCT116 cells stably overexpressing circPHLPP2 (n = 6), (i) Tumor growth curves and final weights in C57 mice bearing MC38 allografts with circPhlpp2 overexpression (n = 7), (j) Tumor growth curves and final weights in BALB/c mice bearing CT26 allografts with circPhlpp2 overexpression (n = 7), and (k and l) Kaplan-Meier survival plots for mice bearing MC38 (n = 8) or CT26 (n = 7) tumors (log-rank test). Statistical tests: two-way ANOVA for panels (a-d) and left panels of (g-j); Student's t-test for panels (e and f) and right panels of (g-j). *P < 0.05, **P < 0.01, ***P < 0.001, ****P < 0.0001.

CircPHLPP2 promotes tumor progression by reducing NK cell infiltration and NK cells' granzyme B and IFN-γ production

Further investigation into how circPHLPP2 affects the tumor immune landscape was conducted through multicolor flow cytometry on harvested tumor tissues. These experiments showed that genetic silencing of circPhlpp2 in MC38 and CT26 models substantially increased the abundance of intratumoral NK cells **(Figures 3a and 3b)**. While B cell proportions were modestly altered in MC38 tumors upon circPhlpp2 knockdown, no such change occurred in CT26 tumors **(Figure 3c)**. Other immune cell subsets remained largely unaffected, underscoring a selective regulatory effect on NK cells.

Since NK cells constitute a primary line of defense in innate antitumor immunity, additional analyses examined their distribution. circPhlpp2 knockdown not only elevated NK cell levels within tumors but also increased their frequency in peripheral blood **(Figure 3d)**. This finding suggests a systemic effect in which circPHLPP2 limits NK cell availability for tumor infiltration by decreasing their circulation. Supporting immunohistochemical staining confirmed greater NK cell (NKp46+) infiltration in tumors following circPhlpp2 depletion **(Figure 3e)**. Moreover, loss of circPhlpp2 enhanced the expression of critical effector molecules—granzyme B and IFN-γ—within tumor-resident NK cells **(Figures 3f and 3g)**, revealing that circPHLPP2 normally restrains the cytotoxic potential of these cells.

To establish whether NK cells mediate the protumorigenic function of circPHLPP2, NK cell depletion was performed using anti-Asialo-GM1 or anti-NK1.1 antibodies before tumor cell injection. This intervention largely negated the antitumor benefit conferred by circPhlpp2 knockdown **(Figure 3h)**. The incomplete reversal noted in MC38 tumors implies that circPHLPP2 may engage additional pathways beyond NK cell regulation to drive tumor growth **(Figure 3h)**. Overall, in both MSI-H and MSS colorectal tumors, circPhlpp2 contributes to immune escape by suppressing NK cell recruitment into the tumor microenvironment and attenuating their production of granzyme B and IFN-γ, thereby accelerating tumor development. In contrast, suppression of circPhlpp2 enhances NK cell infiltration and augments cytotoxic cytokine output, strengthening the host's antitumor immune response.

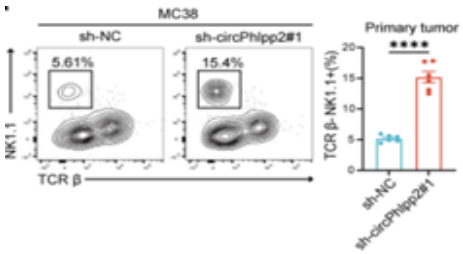

a)

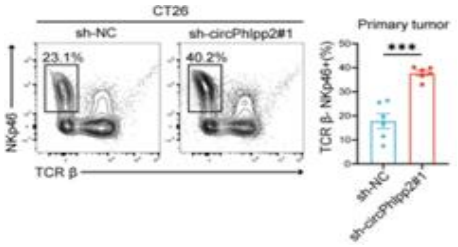

b)

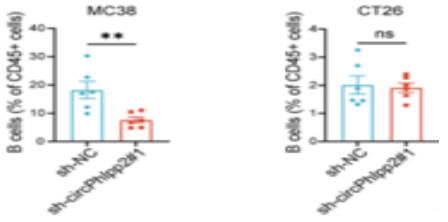

c)

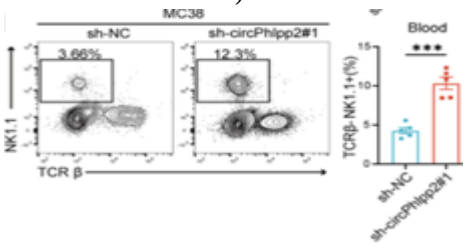

d)

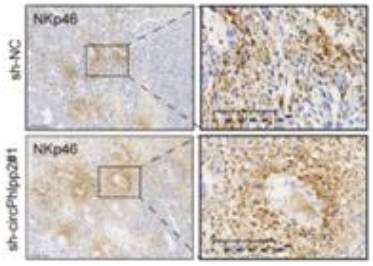

e)

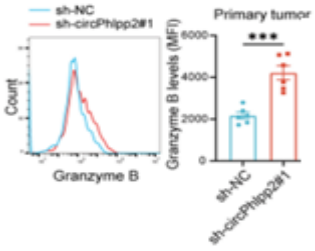

f)

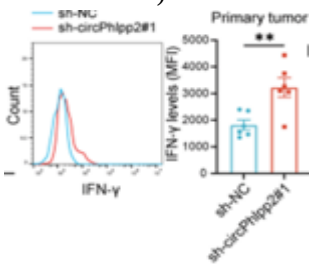

g)

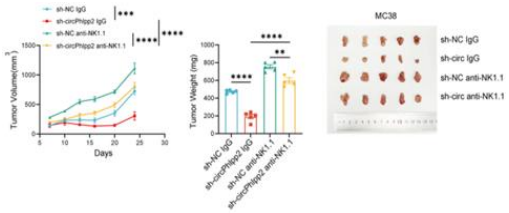

h)

Figure 3. circPHLPP2 reduces NK cell proportion and granzyme B and IFN-γ expression

(a-b) Typical flow cytometry plots (left) and quantitative summaries (right) of NK cell populations in tumors from C57 (a) or BALB/c (b) mice with or without circPhlpp2 knockdown (n = 6), (c) Proportion of B cells in tumors from C57 (left) or BALB/c (right) mice with or without circPhlpp2 knockdown, assessed by flow cytometry (n = 6), (d) Representative plots (left) and quantitative data (right) for circulating NK cells in the blood of tumor-bearing C57 mice with or without circPhlpp2 knockdown (n = 5), (e) Representative IHC staining images for NKp46-positive NK cells in tumors from C57 mice with or without circPhlpp2 knockdown (scale bar = 400 μm), (f and g) Levels of granzyme B (f) and IFN-γ (g) expression in tumor-infiltrating NK cells from C57

mice with or without circPhlpp2 knockdown (n = 6), and (h) Tumor volume, weight, and gross images of allografts in NK cell-depleted versus control C57 mice (n = 5) (left: two-way ANOVA; middle: one-way ANOVA). Data in a-d and f-g were evaluated using Student's t-test. **P < 0.01, ***P < 0.001, ****P < 0.0001.

IL36γ is a functional downstream mediator for circPHLPP2

RNA sequencing was performed on HCT116 cells stably transduced with a lentivirus encoding circPHLPP2 or an empty vector control to identify downstream molecular targets (Additional file 6). Pathway enrichment analysis using KEGG databases showed prominent enrichment in the cytokine-cytokine receptor interaction pathway among genes modulated by circPHLPP2 **(Figure 4a)**. Key differentially expressed genes within this pathway included IL36γ, CCL5, IFNE, and GDF7 **(Figure 4b)**. Subsequent correlation studies in TCGA-COAD and TCGA-READ cohorts identified a strong inverse relationship between IL36γ expression and NK cell abundance, implicating IL36γ as a potential effector of circPHLPP2 in the tumor microenvironment. RT-qPCR validation of candidate cytokines in HCT116 and SW480 cells with circPHLPP2 overexpression revealed consistent upregulation of IL36γ across both lines, despite variable changes in other cytokines **(Figure 4c)**. Western blotting corroborated these transcriptional findings at the protein level: circPHLPP2 overexpression increased IL36γ abundance. At the same time, its depletion decreased IL36γ levels in human CRC cells **(Figures 4d and 4f)**. Parallel results were obtained in murine CRC cell models. These data collectively indicate that circPHLPP2 positively regulates IL36γ expression at the transcriptional level.

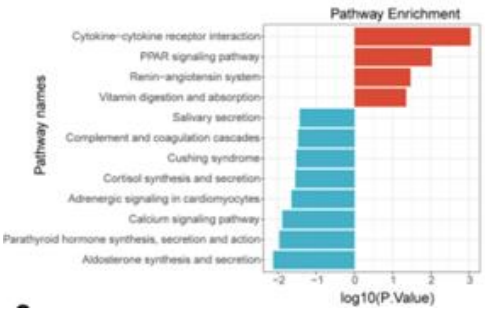

a)

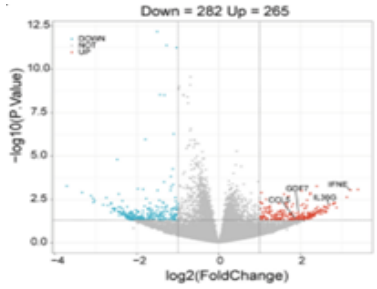

b)

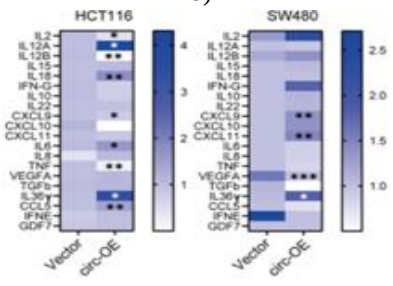

c)

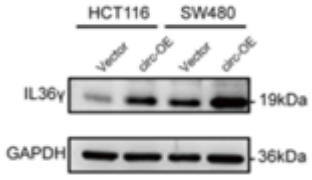

d)

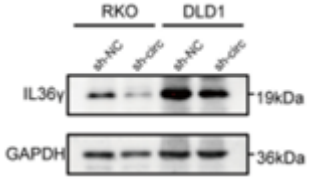

e)

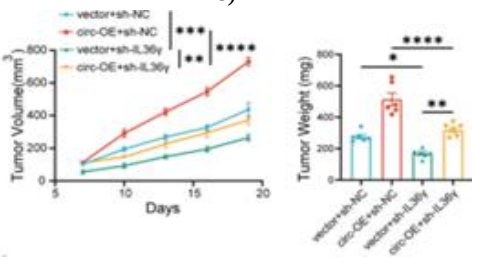

f)

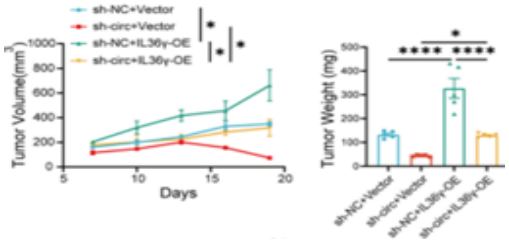

g)

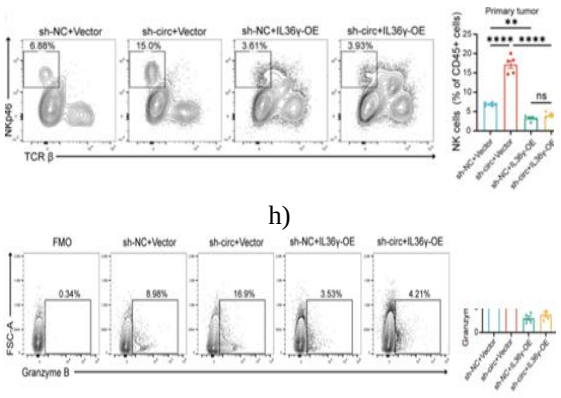

Figure 4. IL36γ is a functional downstream mediator for circPHLPP2

(a) KEGG pathway enrichment analysis performed on differentially expressed mRNAs. DEGs were defined using the limma package in R with cutoffs of |log2 (fold change)| > 1 and p-value < 0.05, (b) Volcano plot highlighting upregulated and downregulated genes, with members of the cytokine-cytokine receptor interaction pathway specifically labeled, (c) Heatmap illustrating relative mRNA expression of selected cytokines in HCT116 and SW480 cells following circPHLPP2 overexpression or vector control, determined by RT-qPCR and normalized to the vector group, (d and e) Representative Western blots depicting IL36γ protein expression after circPHLPP2 overexpression (d) or knockdown (e) in human CRC cells, (f) Tumor volume (left) and weight (right) of subcutaneous allografts in C57 mice inoculated with MC38 cells subjected to circPhlpp2 overexpression combined with IL36γ knockdown (n = 5), (g) Tumor volume (left) and weight (right) of subcutaneous allografts in C57 mice inoculated with MC38 cells subjected to circPhlpp2 knockdown combined with IL36γ overexpression (n = 5), (h) Representative flow cytometry plots (left) and quantitative summary (right) of NK cell frequencies in tumors from C57 mice with circPhlpp2 knockdown or IL36γ overexpression (n = 5), (i) Granzyme B levels in tumor-infiltrating NK cells from C57 mice with circPhlpp2 knockdown or IL36γ overexpression, as measured by flow cytometry (n = 5). Two-way ANOVA analyzed data in the left panels of (f and g). Data in the right panels of (f-i) were analyzed by one-way ANOVA. *P < 0.05, **P < 0.01, ***P < 0.001, ****P < 0.0001.

Prior research has established that IL36γ is overexpressed in CRC tissues and linked to adverse clinical outcomes. This cytokine triggers the release of multiple inflammatory factors, profoundly influencing the immune microenvironment [28]. Survival analyses in the present study confirmed that elevated IL36γ expression predicts poorer overall survival in CRC patients. In vivo, forced IL36γ expression accelerated MC38 tumor growth and reduced NK cell infiltration into tumors. These observations reveal functional parallels between IL36γ and circPHLPP2 in driving CRC advancement.

Rescue experiments were then performed to test whether IL36γ mediates the effects of circPHLPP2. Silencing IL36γ effectively counteracted the tumor-promoting activity induced by circPhlpp2 overexpression **(Figurre 4f)**. Reciprocally, restoring IL36γ expression in circPhlpp2-knockdown cells reversed the inhibition of tumor growth, restored NK cell suppression, and normalized granzyme B and IFN-γ production **(Figures 4g-4i)**. These findings establish that circPHLPP2 promotes colorectal cancer progression largely by upregulating IL36γ.

CircPHLPP2 promotes the transcription of IL36γ via its association with ILF3

We subsequently investigated the mechanism underlying circPHLPP2's regulatory effect on IL36γ transcription. According to the Circinteractome database (https://circinteractome.nia.nih.gov/), circPHLPP2 possesses several miRNA recognition sites; however, it shows no interaction with AGO2, the key protein responsible for guiding miRNAs to complementary sequences in target mRNAs [29]. This observation prompted us to hypothesize that circPHLPP2 operates mainly through direct protein interactions. To test this, we performed MS2-tagged RNA pull-down experiments to isolate proteins associated with circPHLPP2. The assay demonstrated effective enrichment of the MCP-GST capture protein, and circPHLPP2 itself was abundantly recovered in the pulled-down material, confirming the reliability and specificity of the procedure. Mass spectrometry results (Additional file 7) showed that HNRNPC was the most abundant protein. Yet, this factor is well known to interact with many circRNAs and primarily influences their splicing and maturation, suggesting that its association with circPHLPP2 is unlikely to be specific. We therefore conducted FISH studies on the second-most-enriched protein, ILF3, and the third-most-enriched, PABPC1. These experiments showed clear co-localization of ILF3

with circPHLPP2. Forced expression of circPHLPP2 enhanced the nuclear abundance of ILF3 **(Figure 5a)**. Pull-down experiments using plasmids expressing circPHLPP2-MS2 together with MCP-GST produced marked enrichment of ILF3 compared with control conditions **(Figure 5b)**. Consistent with this, RIP assays using an anti-ILF3 antibody specifically recovered circPHLPP2 from CRC cell lysates **(Figure 5c)**. Together, these data confirmed a direct interaction between circPHLPP2 and ILF3. The mass spectrometry profile confirming ILF3 identity is displayed in **Figure 5d**. Complementary nuclear-cytoplasmic fractionation experiments further demonstrated increased nuclear ILF3 protein levels upon circPHLPP2 overexpression **(Figure 5e)**.

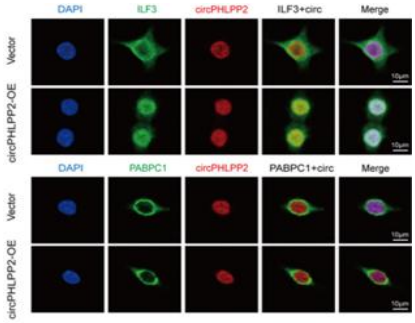

a)

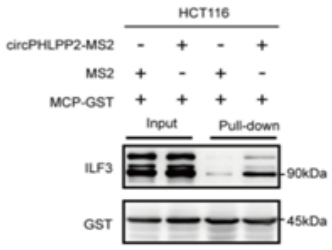

b)

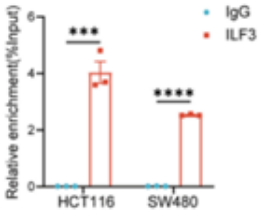

c)

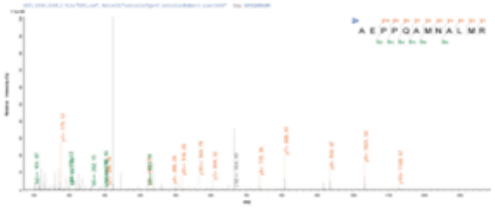

d)

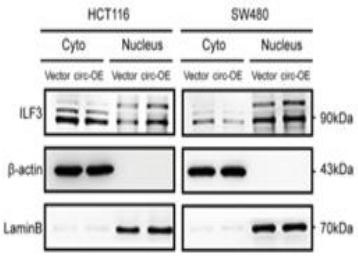

e)

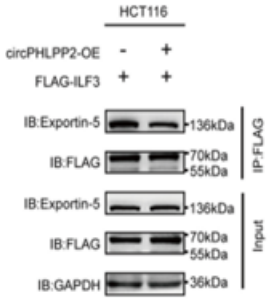

f)

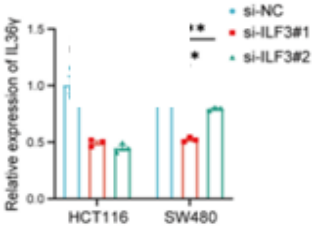

g)

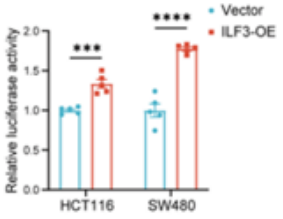

h)

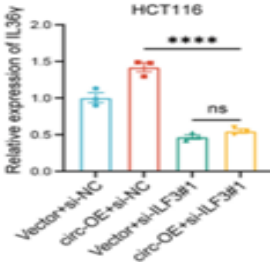

i)

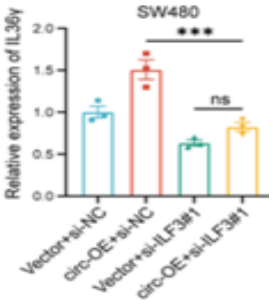

j)

Figure 5. CircPHLPP2 promotes IL36γ transcription through binding to ILF3

(a) Assessment of co-localization between circPHLPP2 and ILF3 (or PABPC1) in HCT116 cells by combined RNA-FISH and immunofluorescence staining (scale bar = 10 μm), (b) Confirmation of circPHLPP2–ILF3 interaction by RNA pull-down assay employing the MS2-tagging approach, (c) RIP assay performed with anti-ILF3 antibody or control IgG in HCT116 and SW480 cells, followed by RT-qPCR analysis of circPHLPP2 enrichment, (d) Mass spectrometry spectrum identifying ILF3, (e) Western blot analysis showing cytoplasmic and nuclear ILF3 protein levels in HCT116 and SW480 cells in the presence or absence of circPHLPP2 overexpression, (f) Coimmunoprecipitation (Co-IP) coupled with Western blotting to evaluate the association between ILF3 and exportin-5 in circPHLPP2-overexpressing versus control HCT116 cells, (g) Relative IL36γ mRNA levels determined by RT-qPCR in HCT116 and SW480 cells following transfection with si-ILF3#1, si-ILF3#2, or si-NC, (h) Relative luciferase activity (FL/RL) measured in HCT116 and SW480 cells after co-transfection with the IL36γ promoter luciferase reporter and either an ILF3 overexpression plasmid or empty control vector, and (i and j) Relative IL36γ expression quantified by RT-qPCR in HCT116 (i) and SW480 (j) cells under conditions of circPHLPP2 overexpression alone or combined with ILF3 knockdown. Statistical analysis for panels (c and h) used Student's t-test. Data in panels (g, i and j) were evaluated by one-way ANOVA. ***P < 0.001, ****P < 0.0001

ILF3 (also designated NF90/NF110) encodes a dsRNA-binding protein capable of forming multiprotein complexes with mRNAs, small noncoding RNAs, and other dsRNAs, thereby controlling gene expression and enhancing mRNA stability [30]. Its functional activity is strongly influenced by its intracellular distribution [31]. Functioning as a nucleocytoplasmic shuttling factor, ILF3 is exported from the nucleus through exportin-5; however, RNA-bound ILF3 is resistant to this export process [32]. Earlier studies have shown that complex formation between ILF3 and specific circRNAs can alter ILF3 localization and modulate immune responses [33]. Based on these insights, we hypothesized that circPHLPP2 competes with ILF3 for binding to exportin-5, thereby reducing ILF3–exportin-5 association and leading to nuclear retention of ILF3. Co-IP experiments validated this model by showing that elevated circPHLPP2 levels diminished the interaction between ILF3 and exportin-5 **(Figure 5f)**. Structurally, ILF3 includes a nuclear localization signal, two dsRNA-binding domains (dsRBDs), an RGG motif, and a C-terminal arginine/glycine-rich region [34]. Prior evidence established that exportin-5 engages the dsRBDs of ILF3 to facilitate nuclear export, and that occupancy of these domains by dsRNA blocks exportin-5 binding [32]. Accordingly, we proposed that circPHLPP2 engages the dsRBDs of ILF3, thereby interfering with exportin-5 recruitment. Supporting this, GST pull-down assays revealed that removal of the dsRBDs segment from ILF3 (ILF3 △d) completely abolished binding to circPHLPP2. Considering the observed nuclear co-localization of circPHLPP2 and ILF3, we next examined whether ILF3 directly influences IL36γ transcription. Two distinct siRNAs were used to silence ILF3. Both siILF3#1 and siILF3#2 efficiently suppressed ILF3 mRNA expression relative to scramble control and led to a marked reduction in IL36γ transcript levels in CRC cells **(Figure 5g)**. Promoter-driven luciferase reporter assays further revealed that ILF3 overexpression significantly elevated luciferase activity compared with control vector **(Figure 5h)**. These observations indicate that ILF3 acts as a positive regulator of IL36γ transcription in CRC cells. Importantly, depletion of ILF3 largely abolished the upregulation of IL36γ mRNA induced by circPHLPP2 overexpression **(Figures 5i and 5j)**, demonstrating that the transcriptional effect of circPHLPP2 on IL36γ depends on ILF3. In summary, the presented results demonstrate that circPHLPP2 drives IL36γ transcription by forming a complex with ILF3.

Knockdown of circPHLPP2 augments the therapeutic efficacy of anti-PD-1 blockade in vivo

The present data showed that circPHLPP2 drives CRC cell growth in vivo, and that its depletion relieves the

inhibitory effect on NK cells, thereby bolstering systemic anti-tumor immunity. We therefore investigated whether targeting circPHLPP2 could sensitize tumors to anti-PD-1 immunotherapy. Experiments were conducted to compare the individual and combined effects of circPhlpp2 silencing, anti-PD-1 administration, and their combination on tumor development in syngeneic immunocompetent mouse models. In the MC38 model, which mimics MSI-H colorectal cancer and exhibits strong responsiveness to immune checkpoint blockade [35], anti-PD-1 monotherapy slowed tumor advancement, yet circPhlpp2 knockdown produced superior suppression of tumor progression compared with anti-PD-1 treatment alone **(Figures 6a-6c)**. By contrast, in the CT26 model, which corresponds to the MSS subtype known for primary resistance to immunotherapy [36], anti-PD-1 therapy failed to exert a meaningful effect, as predicted, whereas circPhlpp2 knockdown showed a clear tendency to restrain tumor expansion **(Figures 6d-6f)**. Notably, combining anti-PD-1 treatment with circPhlpp2 knockdown resulted in significantly greater tumor control than anti-PD-1 treatment in control groups across both models, with the most pronounced improvement observed in tumor volume **(Figures 6a and 6d)**. These observations indicate that loss of circPHLPP2 substantially enhances the antitumor activity of anti-PD-1 therapy.

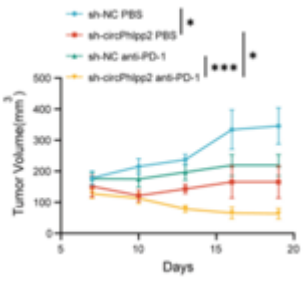

a)

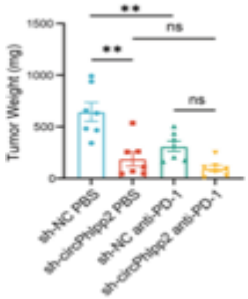

b)

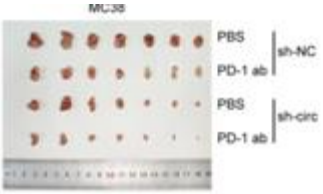

c)

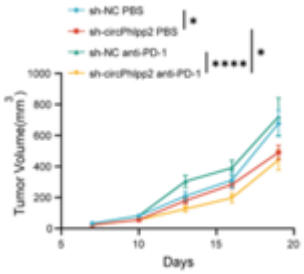

d)

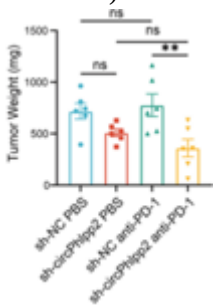

e)

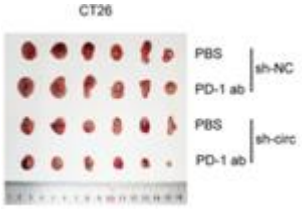

f)

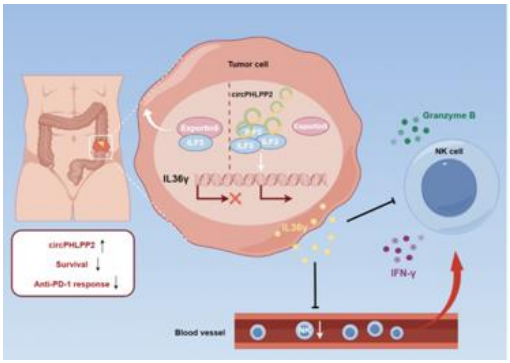

g)

Figure 6. Knockdown of circPHLPP2 augments the efficacy of anti-PD-1 treatment in vivo

(a-c) Growth curves showing tumor volume (a) and final tumor weight (b) in C57 mice after subcutaneous

implantation of MC38 cells stably expressing control or circPhlpp2-targeting shRNA. Tumors were collected and imaged following anti-PD-1 antibody treatment (c) (n = 7), (d-f) Tumor volume (d) and tumor weight (e) in BALB/c mice bearing subcutaneous CT26 tumors with or without circPhlpp2 knockdown. Tumors were excised and photographed after anti-PD-1 therapy (f) (n = 6), (g) Proposed working model depicting how circPHLPP2 accelerates CRC progression by elevating IL36γ levels via direct interaction with ILF3, leading to impaired NK cell recruitment and decreased expression of granzyme B and IFN-γ within NK cells. Suppression of circPHLPP2 has the potential to improve the clinical outcomes of anti-PD-1 therapy in CRC (created with Figdraw). Data presented in panels (a) and (d) were analyzed using two-way ANOVA. Data in panels (b) and (c) were analyzed using one-way ANOVA.*P < 0.05, **P < 0.01, ***P < 0.001, ****P < 0.0001

Cancer immunotherapy has demonstrated encouraging antitumor activity across multiple malignancies, including colorectal cancer. Nevertheless, therapeutic resistance remains a major challenge, especially in patients with microsatellite-stable (MSS) or proficient mismatch repair (pMMR) CRC [37]. Accumulating evidence indicates that circular RNAs are involved in tumor development [38], and some circRNAs show associations with clinical responses to anti-PD-1 treatment [39]. Investigating circRNAs that shape the tumor immune microenvironment may uncover novel biomarkers to predict immunotherapy outcomes and identify new therapeutic targets. In the current study, we established that circPHLPP2 correlates with anti-PD-1 resistance in patients with advanced MSS/pMMR CRC and provide the first description of its mechanistic role in immune evasion. Furthermore, our findings offer a mechanistic basis for improving anti-PD-1 therapeutic efficacy in CRC.

Analysis of circPHLPP2 expression in CRC patients receiving anti-PD-1-based regimens revealed significantly elevated levels in tumor tissues relative to adjacent normal tissues. Expression was further increased in individuals exhibiting resistance to anti-PD-1 therapy. Moreover, patients with high circPHLPP2 expression displayed poorer overall survival, supporting its potential contribution to tumor progression. Functional assays showed that circPHLPP2 has minimal effect on CRC cell proliferation in vitro. However, it substantially promoted tumor growth in both immunodeficient nude mice and immunocompetent syngeneic models, implying a primary role in modulating interactions between tumor cells and the immune system. Specifically, circPhlpp2 reduced NK cell abundance in peripheral blood and tumor tissues while decreasing granzyme B and IFN-γ production in NK cells, thereby promoting immune escape. Given that NK cells can eliminate tumor targets via antibody-dependent cellular cytotoxicity and other pathways, additional research is required to clarify the broader effects of circPhlpp2 on NK cell biology beyond cytokine secretion. Although T cells represent the principal effectors of checkpoint inhibitor efficacy, interference with CTLA-4 or PD-1 signaling can also augment NK cell-mediated antitumor activity [40]. Consistent with this concept, prior work has shown that circUHRF1 contributes to anti-PD-1 resistance by impairing NK cell function in hepatocellular carcinoma [41]. Collectively, these observations underscore the importance of circPHLPP2 in driving resistance to anti-PD-1 therapy in MSS/pMMR advanced CRC through its effects on NK cells. Our results further indicate that inhibiting circPHLPP2 improves anti-PD-1 responses in CRC and position circPHLPP2 as a promising therapeutic target.

Earlier investigations have shown that circRNAs can promote either immune activation or suppression by modulating cytokines and chemokines. For instance, circCYP24A1 alters the tumor microenvironment by enhancing CCL5 secretion [42]. In the present work, pathway analysis linked circPHLPP2 to the cytokine–cytokine receptor interaction network, with IL36γ identified as a key downstream effector. IL36γ has been implicated in the progression and metastatic spread of multiple cancer types. In non-small cell lung cancer, it supports tumor growth by increasing glutathione synthesis and protecting cells from oxidative stress-induced death [43]. In the colon, IL-36γ exacerbates inflammation and tumorigenesis by altering cell-matrix adhesion and activating Wnt signaling [28]. Clinical data have also associated high IL-36α and IL-36β levels, or high IL-36α with low IL-36γ, with improved survival in CRC, suggesting prognostic value. These reports align with our observation that IL36γ promotes CRC development. However, the immunomodulatory functions of IL-36γ appear context-dependent. While one study found that IL-36γ stimulates antitumor immunity in melanoma by boosting IFN-γ production from $CD8^+$ T cells and NK cells [44], another described a pathogenic role in colitis through suppression of

regulatory T cell differentiation and enhancement of Th9 responses [45]. Our experiments confirmed that IL36γ recapitulates the effects of circPhlpp2 by accelerating CRC cell growth and suppressing NK cell infiltration and effector molecule expression. Moreover, IL36γ overexpression reversed the phenotypes caused by circPhlpp2 knockdown. We therefore propose that circPhlpp2 contributes to CRC progression, at least in part, through IL36γ secretion, with the net impact of IL36γ on tumor behavior likely varying across tissues and disease contexts.

Circular RNAs are known to function as miRNA sponges, interact with RNA-binding proteins, and, in some cases, encode peptides. Their activity is heavily influenced by subcellular localization [46]. Nuclear-localized circRNAs participate in transcriptional control, alternative splicing, and chromatin organization [38]. In our study, FISH analysis confirmed predominant nuclear localization of circPHLPP2. We further demonstrated that circPHLPP2 directly binds ILF3, thereby retaining ILF3 in the nucleus. Nuclear export of ILF3 requires association with exportin-5, a process that RNA binding can disrupt [32]. Our data showed that circPHLPP2–ILF3 complex formation reduces ILF3 interaction with exportin-5, thereby increasing nuclear ILF3 abundance. ILF3 has been linked to cancer pathogenesis, progression, therapy resistance, and prognosis in diverse malignancies [30, 47, 48]. Through its capacity to bind DNA and RNA, ILF3 regulates transcription, translation, mRNA stability, and pri-miRNA processing [49, 50]. Nuclear ILF3 can modulate the expression of specific genes, including TGF-β2 and uPA [47, 51]. Our findings establish that nuclear ILF3 enhances IL36γ transcription and that the circPHLPP2–ILF3 interaction promotes ILF3 nuclear accumulation, culminating in elevated IL36γ levels.

Several limitations should be acknowledged. First, the relatively small patient cohort necessitates validation in larger, independent cohorts. Second, the precise pathways through which IL36γ controls NK cell infiltration and function remain incompletely defined and require further elucidation. Third, murine models cannot fully replicate the human tumor immune microenvironment, highlighting the need for confirmatory studies in humanized mouse systems.

Conclusion

In summary, circPHLPP2 accelerates CRC progression by remodeling the tumor microenvironment. Mechanistically, it upregulates IL36γ expression via direct interaction with ILF3, leading to decreased NK cell infiltration and reduced production of granzyme B and IFN-γ in NK cells **(Figure 6g)**. These results suggest that therapeutic targeting of circPHLPP2 may improve the clinical efficacy of anti-PD-1 therapy in patients with CRC.

Acknowledgments: None

Conflict of Interest: None

Financial Support: None

Ethics Statement: None

References

1. Sung H, Ferlay J, Siegel RL, Laversanne M, Soerjomataram I, Jemal A, et al. Global Cancer statistics 2020: GLOBOCAN estimates of incidence and Mortality Worldwide for 36 cancers in 185 countries. CA Cancer J Clin. 2021;71:209-49.
2. Guo S, Sun Y. OTOP2, inversely modulated by miR-3148, inhibits CRC Cell Migration, Proliferation and epithelial-mesenchymal transition: evidence from Bioinformatics Data Mining and Experimental Verification. Cancer Manag Res. 2022;14:1371-84.
3. Diaz LA Jr., Shiu KK, Kim TW, Jensen BV, Jensen LH, Punt C, et al. Pembrolizumab versus chemotherapy for microsatellite instability-high or mismatch repair-deficient metastatic colorectal cancer (KEYNOTE-177): final analysis of a randomised, open-label, phase 3 study. Lancet Oncol. 2022;23:659-70.
4. He X, Xu C. Immune checkpoint signaling and cancer immunotherapy. Cell Res. 2020;30:660-9.
5. Manca P, Corti F, Intini R, Mazzoli G, Miceli R, Germani MM, et al. Tumour mutational burden as a biomarker in patients with mismatch repair deficient/microsatellite instability-high metastatic colorectal cancer treated with immune checkpoint inhibitors. Eur J Cancer. 2023;187:15-24.
6. Fukuoka S, Hara H, Takahashi N, Kojima T, Kawazoe A, Asayama M, et al. Regorafenib Plus Nivolumab in patients with Advanced gastric or colorectal Cancer: an Open-Label, Dose-Escalation,

and dose-expansion phase ib trial (REGONIVO, EPOC1603). J Clin Oncol. 2020;38:2053-61.
7. Zhou WY, Cai ZR, Liu J, Wang DS, Ju HQ, Xu RH. Circular RNA: metabolism, functions and interactions with proteins. Mol Cancer. 2020;19:172.
8. Long F, Lin Z, Li L, Ma M, Lu Z, Jing L, et al. Comprehensive landscape and future perspectives of circular RNAs in colorectal cancer. Mol Cancer. 2021;20:26.
9. Ju HQ, Zhao Q, Wang F, Lan P, Wang Z, Zuo ZX, et al. A circRNA signature predicts postoperative recurrence in stage II/III colon cancer. EMBO Mol Med. 2019;11:e10168.
10. Huang M, Peng X, Yang L, Yang S, Li X, Tang S, et al. Non-coding RNA derived from extracellular vesicles in cancer immune escape: Biological functions and potential clinical applications. Cancer Lett. 2021;501:234-46.
11. Ma Z, Shuai Y, Gao X, Wen X, Ji J. Circular RNAs in the tumour microenvironment. Mol Cancer. 2020;19:8.
12. Hu Z, Chen G, Zhao Y, Gao H, Li L, Yin Y, et al. Exosome-derived circCCAR1 promotes CD8+ T-cell dysfunction and anti-PD1 resistance in hepatocellular carcinoma. Mol Cancer. 2023;22:55.
13. Chen DL, Sheng H, Zhang DS, Jin Y, Zhao BT, Chen N, et al. The circular RNA circDLG1 promotes gastric cancer progression and anti-PD-1 resistance through the regulation of CXCL12 by sponging miR-141-3p. Mol Cancer. 2021;20:166.
14. Shimasaki N, Jain A, Campana D. NK cells for cancer immunotherapy. Nat Rev Drug Discov. 2020;19:200-18.
15. Voskoboinik I, Smyth MJ, Trapani JA. Perforin-mediated target-cell death and immune homeostasis. Nat Rev Immunol. 2006;6:940-52.
16. Fauriat C, Long EO, Ljunggren HG, Bryceson YT. Regulation of human NK-cell cytokine and chemokine production by target cell recognition. Blood. 2010;115:2167-76.
17. López-Soto A, Gonzalez S, Smyth MJ, Galluzzi L. Control of Metastasis by NK Cells. Cancer Cell. 2017;32:135-54.
18. Hsu J, Hodgins JJ, Marathe M, Nicolai CJ, Bourgeois-Daigneault MC, Trevino TN, et al. Contribution of NK cells to immunotherapy mediated by PD-1/PD-L1 blockade. J Clin Invest. 2018;128:4654-68.
19. Imai K, Matsuyama S, Miyake S, Suga K, Nakachi K. Natural cytotoxic activity of peripheral-blood lymphocytes and cancer incidence: an 11-year follow-up study of a general population. Lancet. 2000;356:1795-9.
20. Melero I, Ochoa MC, Molina C, Sanchez-Gregorio S, Garasa S, Luri-Rey C, et al. Intratumoral co-injection of NK cells and NKG2A-neutralizing monoclonal antibodies. EMBO Mol Med. 2023;15:e17804.
21. Ju HQ, Ying H, Tian T, Ling J, Fu J, Lu Y, et al. Mutant Kras- and p16-regulated NOX4 activation overcomes metabolic checkpoints in development of pancreatic ductal adenocarcinoma. Nat Commun. 2017;8:14437.
22. Lin JF, Hu PS, Wang YY, Tan YT, Yu K, Liao K, et al. Phosphorylated NFS1 weakens oxaliplatin-based chemosensitivity of colorectal cancer by preventing PANoptosis. Signal Transduct Target Ther. 2022;7:54.
23. Zheng R, Zhang K, Tan S, Gao F, Zhang Y, Xu W, et al. Exosomal circLPAR1 functions in colorectal cancer diagnosis and tumorigenesis through suppressing BRD4 via METTL3-eIF3h interaction. Mol Cancer. 2022;21:49.
24. Seymour L, Bogaerts J, Perrone A, Ford R, Schwartz LH, Mandrekar S, et al. iRECIST: guidelines for response criteria for use in trials testing immunotherapeutics. Lancet Oncol. 2017;18:e143-52.
25. Gandara DR, Mack PC, Bult C, Li T, Lara PN Jr., Riess JW, et al. Bridging tumor genomics to patient outcomes through an integrated patient-derived xenograft platform. Clin Lung Cancer. 2015;16:165-72.
26. Kawada M, Inoue H, Kajikawa M, Sugiura M, Sakamoto S, Urano S, et al. A novel monoclonal antibody targeting coxsackie virus and adenovirus receptor inhibits tumor growth in vivo. Sci Rep. 2017;7:40400.
27. Hegde PS, Chen DS. Top 10 challenges in Cancer Immunotherapy. Immunity. 2020;52:17-35.
28. Yang W, Dong HP, Wang P, Xu ZG, Xian J, Chen J, et al. IL-36γ and IL-36Ra reciprocally regulate Colon inflammation and tumorigenesis by modulating the Cell-Matrix Adhesion Network and Wnt signaling. Adv Sci (Weinh). 2022;9:e2103035.
29. Rowley JW, Chappaz S, Corduan A, Chong MM, Campbell R, Khoury A, et al. Dicer1-mediated

miRNA processing shapes the mRNA profile and function of murine platelets. Blood. 2016;127:1743-51.
30. Li K, Wu JL, Qin B, Fan Z, Tang Q, Lu W, et al. ILF3 is a substrate of SPOP for regulating serine biosynthesis in colorectal cancer. Cell Res. 2020;30:163-78.
31. Castella S, Bernard R, Corno M, Fradin A, Larcher JC. Ilf3 and NF90 functions in RNA biology. Wiley Interdiscip Rev RNA. 2015;6:243-56.
32. Brownawell AM, Macara IG. Exportin-5, a novel karyopherin, mediates nuclear export of double-stranded RNA binding proteins. J Cell Biol. 2002;156:53-64.
33. Li X, Liu CX, Xue W, Zhang Y, Jiang S, Yin QF, et al. Coordinated circRNA Biogenesis and function with NF90/NF110 in viral infection. Mol Cell. 2017;67:214-27.
34. Duchange N, Pidoux J, Camus E, Sauvaget D. Alternative splicing in the human interleukin enhancer binding factor 3 (ILF3) gene. Gene. 2000;261:345-53.
35. Bao Y, Zhai J, Chen H, Wong CC, Liang C, Ding Y, et al. Targeting m(6)A reader YTHDF1 augments antitumour immunity and boosts anti-PD-1 efficacy in colorectal cancer. Gut. 2023;72:1497-509.
36. Zhang B, Yao K, Zhou E, Zhang L, Cheng C. Chr20q amplification defines a distinct molecular subtype of microsatellite stable colorectal Cancer. Cancer Res. 2021;81:1977-87.
37. Ganesh K, Stadler ZK, Cercek A, Mendelsohn RB, Shia J, Segal NH, et al. Immunotherapy in colorectal cancer: rationale, challenges and potential. Nat Rev Gastroenterol Hepatol. 2019;16:361-75.
38. Chen LL. The expanding regulatory mechanisms and cellular functions of circular RNAs. Nat Rev Mol Cell Biol. 2020;21:475-90.
39. Jiang W, Pan S, Chen X, Wang ZW, Zhu X. The role of lncRNAs and circRNAs in the PD-1/PD-L1 pathway in cancer immunotherapy. Mol Cancer. 2021;20:116.
40. Guillerey C, Huntington ND, Smyth MJ. Targeting natural killer cells in cancer immunotherapy. Nat Immunol. 2016;17:1025-36.
41. Zhang PF, Gao C, Huang XY, Lu JC, Guo XJ, Shi GM, et al. Cancer cell-derived exosomal circUHRF1 induces natural killer cell exhaustion and may cause resistance to anti-PD1 therapy in hepatocellular carcinoma. Mol Cancer. 2020;19:110.
42. Gu L, Sang Y, Nan X, Zheng Y, Liu F, Meng L, et al. circCYP24A1 facilitates esophageal squamous cell carcinoma progression through binding PKM2 to regulate NF-κB-induced CCL5 secretion. Mol Cancer. 2022;21:217.
43. Wang P, Yang W, Guo H, Dong HP, Guo YY, Gan H, et al. IL-36γ and IL-36Ra reciprocally regulate NSCLC progression by modulating GSH Homeostasis and oxidative stress-Induced cell death. Adv Sci (Weinh). 2021;8:e2101501.
44. Wang X, Zhao X, Feng C, Weinstein A, Xia R, Wen W, et al. IL-36γ transforms the Tumor Microenvironment and promotes type 1 lymphocyte-mediated Antitumor Immune responses. Cancer Cell. 2015;28:296-306.
45. Harusato A, Abo H, Ngo VL, Yi SW, Mitsutake K, Osuka S, et al. IL-36γ signaling controls the induced regulatory T cell-Th9 cell balance via NFκB activation and STAT transcription factors. Mucosal Immunol. 2017;10:1455-67.
46. Liu CX, Chen LL. Circular RNAs: characterization, cellular roles, and applications. Cell. 2022;185:2016-34.
47. Li P, Mi Q, Yan S, Xie Y, Cui Z, Zhang S, et al. Characterization of circSCL38A1 as a novel oncogene in bladder cancer via targeting ILF3/TGF-β2 signaling axis. Cell Death Dis. 2023;14:59.
48. Xiao L, Zhang Y, Luo Q, Guo C, Chen Z, Lai C. DHRS4-AS1 regulate gastric cancer apoptosis and cell proliferation by destabilizing DHX9 and inhibited the association between DHX9 and ILF3. Cancer Cell Int. 2023;23:304.
49. Liu J, Liu ZX, Li JJ, Zeng ZL, Wang JH, Luo XJ, et al. The Macrophage-Associated LncRNA MALR facilitates ILF3 liquid-liquid phase separation to promote HIF1α signaling in Esophageal Cancer. Cancer Res. 2023;83:1476-89.
50. Tan J, Sun M, Yin J, Zhou Q, Zhao R, Chen Q, et al. Hsa_circ_0005050 interacts with ILF3 and affects cell apoptosis and proliferation by disrupting the balance between p53 and p65. Chem Biol Interact. 2022;368:110208.
51. Hu Q, Lu YY, Noh H, Hong S, Dong Z, Ding HF, et al. Interleukin enhancer-binding factor 3 promotes breast tumor progression by regulating sustained urokinase-type plasminogen activator expression. Oncogene. 2013;32:3933-43.